Available online at www.sciencedirect.com
ScienceDirect
Journal of Power Sources 174 (2007) 1263–1269
JOURNAL OF POWER SOURCES
www.elsevier.com/locate/jpowsour

On the performance of graphitized meso carbon microbeads (MCMB)–meso carbon fibers (MCF) and synthetic graphite electrodes at elevated temperatures

Elena Markevich, Elad Pollak, Gregory Salitra, Doron Aurbach *

Department of Chemistry, Bar-Ilan University, 52900 Ramat-Gan, Israel

Available online 30 June 2007

Abstract

The behavior of graphite electrodes comprising either synthetic flakes or round-shaped particles, meso carbon microbeads (MCMB) and meso carbon fibers (MCF), were studied at elevated temperatures (up to 80 °C) in standard solutions of ethylene carbonate–ethylmethylcarbonate (EC–EMC)/$LiPF_6$. Electron microscopy, X-ray diffraction (XRD), and Raman spectroscopy were used in conjunction with standard electrochemical techniques, including impedance spectroscopy. While electrodes comprised of synthetic flakes demonstrated impressive stability, even at 80 °C, MCMB–MCF electrodes demonstrated a rapid capacity fading at elevated temperatures. This capacity fading is due to the formation of thick surface films that contain Li carbonate and Li oxalate as part of their components. The thick surface films are formed upon cycling because of the surface properties of round-shaped graphite particles, as discussed herein. The MCMB–MCF electrodes fail at high temperature because of the high impedance developed due to the formation of thick surface films.

Keywords: Graphite electrodes; MCMB–MCF; Elevated temperature; Raman; EIS; Capacity fading

1. Introduction

High temperature stability is of profound importance for the performance of Li-ion cells, both for portable electronic devices and for electric vehicles. For example, the use of Li-ion batteries for notebook computers and laptops demands their reasonable performance at elevated temperatures, since many electronic devices involve considerable heat evolution during operation. Operating Li-ion batteries at high rates leads to heat dissipation due to the system's internal resistance. The rate of heat generation in Li-ion batteries operating at high rates may be higher than its transport out of the systems, which drives the batteries to work at elevated temperatures. Hence, high cycling performance at elevated temperatures is an essential requirement for all rechargeable battery systems designed for wide applications.

It is known that the stability of Li-ion cells degrades when they are exposed to or operated at temperatures above 60 °C [1–3]. There is a variety of cathode and anode material combinations for Li-ion cells, and in each specific case it is important to know which electrode is primarily responsible for the limitation in cycle life at high temperatures. For example, it has been shown for the $LiNi_{0.8}Co_{0.15}Al_{0.05}O_2$/($LiPF_6$-EC/DEC)/natural graphite system [3,4], both at ambient and at elevated temperatures, that the cathode side is responsible for the impedance growth and capacity fading observed upon cycling of these systems. Similarly, the interfacial resistance of the positive electrode has been demonstrated as the main reason for the impedance rise upon cycling $LiNi_{0.8}Co_{0.2}O_2$/($LiPF_6$-EC/DEC)/MCMB cells at elevated temperatures [5].

Zhang et al. [6] has shown, with respect to the $LiCoO_2$/carbon system (Sony US 18650S cells), that the electrodes' interfacial resistance growth with cycling is the major cause for capacity loss. The $LiCoO_2$ electrodes were found to contribute more to the total resistance of the full cells than the other components (i.e., the negative electrodes, solutions, and the electrical contacts) and also to the capacity decay of $LiCoO_2$/graphite cells at ambient temperature. However, at elevated temperatures, e.g., 50–55 °C, cycled $LiCoO_2$/graphitized carbon cells exhibited a higher negative electrode resistance [7,8]. A drastic increase in the negative electrode resistance, together with an increase of active lithium losses in the system due to side reactions at the

* Corresponding author. Tel.: +972 3 531 8317; fax: +972 3 535 1250.
E-mail address: aurbach@mail.biu.ac.il (D. Aurbach).

0378-7753/$ – see front matter © 2007 Elsevier B.V. All rights reserved.
doi:10.1016/j.jpowsour.2007.06.187

anode, seem to be the main reasons for the capacity fading of $LiCoO_2$/graphite cells at elevated temperatures in this case.

There are several types of graphite materials that may be suitable for Li-ion battery application. Natural graphite usually appears as flakes, due to its natural, layered structure. Synthetic graphite is also available in micron-size flakes [9]. However, the flaky morphology is not good for the kinetics of composite graphite electrodes, because these flakes are oriented with the basal planes in parallel to the current collector, so that the edge planes through which Li-ions intercalate, have only a limited access to the solution [10]. Because of that, round-shaped graphite particles have been developed. These include meso carbon microbeads (MCMB), which are micron size graphite balls, and chopped graphite fibers, or meso carbon fibers (MCF) [11]. Using such particles eliminates the problems of contact between the solution and the edge planes of the graphite particles in the composite negative electrodes.

In the present study, we observed the cycling behavior and capacity fading mechanisms of two types of graphite electrodes: in one type, the active mass comprised round-shaped particles, MCMB and MCF, while the other type consisted of micronic-size synthetic graphite flakes. Raman spectroscopy, XRD, and electron microscopy were used in conjunction with standard electrochemical techniques, including impedance spectroscopy.

2. Experimental

Composite MCMB + MCF (meso carbon microbeads + chopped meso carbon fibers) electrodes on copper foil current collectors (94% of active material, containing 40 wt.% MCMB and 60% MCF) and $LiCoO_2$ (95%) on aluminum foil (one-side loading) were obtained from LG Chem. Composite electrodes comprised of 90% KS15 (Timcal) synthetic graphite flakes and 10% PVdF binder were prepared as described previously [12]. In general, the graphite electrodes' load was usually 5 mg cm^{-2} for KS15 graphite electrodes, and 9 mg cm^{-2} for MCMB + MCF electrodes. The electrolyte solution for this study was 1 M $LiPF_6$ in ethylene carbonate (EC) + ethylmethylcarbonate (EMC) 1:2 mixture, Li-battery grade, from Merck KGaA.

Galvanostatic cycling was carried out in coin-type cells (model 2032, standard products from NRC, Canada) with a Maccor Inc., model 2000, multichannel battery tester. For impedance measurements, three-electrode coin-type cells were assembled, as already described [13]. Impedance measurements and potentiodynamic polarizations were performed with a computerized potentiostat–galvanostat model 20 Autolab, which included a FRA module from Eco Chemie (Netherlands).

Specific surface area measurements were conducted with the use of Autosorb1 (Quantochrome, Inc.), using nitrogen as an adsorbate (BET approach). The structure of the electrodes was determined by X-ray diffraction (XRD). XRD patterns were recorded with a BRUKER-AXS, D8-Advance diffractometer using Cu $K\alpha_1$ radiation. Raman spectra were measured ex situ in a back-scattered configuration through optical glass windows in hermetically closed cells, using a micro-Raman spectrometer HR800 (Jobin Yvon Horiba), holographic grating 1800 grooves/mm, with an He–Ne laser (excitation line 632.8 nm, 0.9 mW), objective 50× (numerical aperture 0.75). The morphology of the electrodes was examined by scanning electron microscopy (SEM) with a JEOL-JSM 840 microscope.

3. Results and discussion

In parallel, we tested MCMB/MCF electrodes in cells that also contained $LiCoO_2$ electrodes, the most commonly used positive electrodes in Li-ion cells, and two half cells: MCMB + MCF/Li and $LiCoO_2$/Li (same temperature and cycling rate, Fig. 1a). A typical comparison of cycling data from three parallel experiments in MCMB–MCF/$LiCoO_2$, Li/$LiCoO_2$, and Li/MCMB–MCF cells (Fig. 1a) indicates that the capacity fading of the carbon electrodes at elevated temperature upon cycling is more pronounced than that of $LiCoO_2$ cathodes. In order to estimate the contribution of the positive and the negative electrodes to the total capacity fading of full cells, the following post-mortem analysis was carried out: MCMB–MCF/$LiCoO_2$ cells were cycled at 60 °C until their end

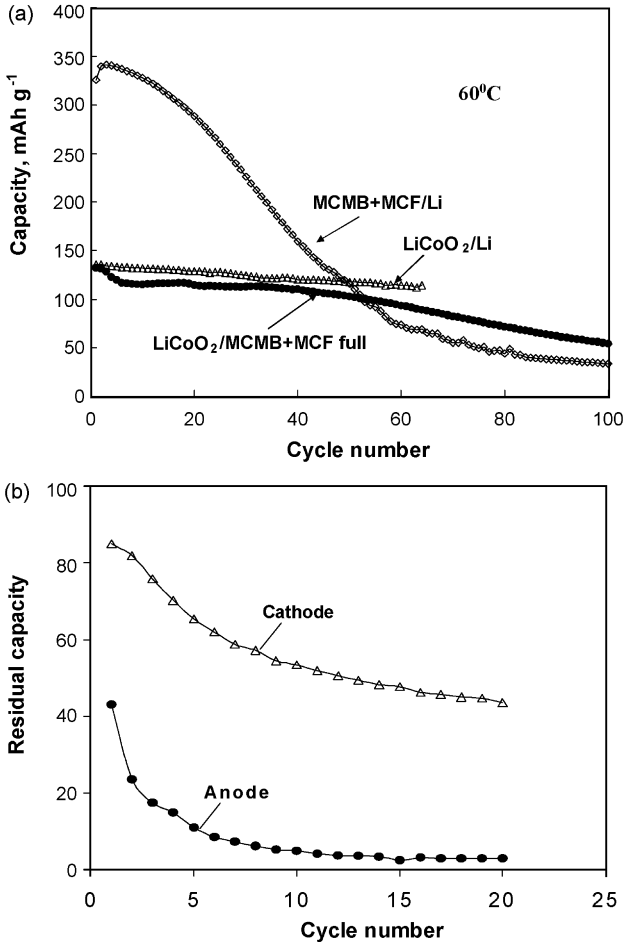

Fig. 1. (a) Results (capacity vs. cycle number) from galvanostatic cycling of a $LiCoO_2$/MCMB + MCF cell and two half cells: MCMB + MCF/Li and $LiCoO_2$/Li in 1 M $LiPF_6$/EC–EMC at a *C*/8 rate and at 60 °C. (b) Results from galvanostatic cycling of two half cells: $LiCoO_2$/Li ("cathode") and MCMB + MCF/Li ("anode") at 60 °C. The working electrodes of both cells ($LiCoO_2$ and MCMB + MCF) were taken out of a full $LiCoO_2$/MCMB + MCF cells, which were cycled for 200 cycles at 60 °C, lost their capacity, and were then disassembled (post-mortem analysis).

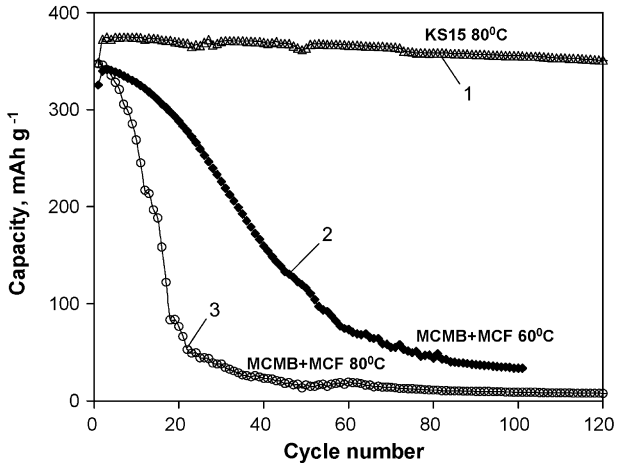

Fig. 2. Results (capacity vs. cycle number) from galvanostatic cycling of three graphite/Li cells at elevated temperatures in 1 M $LiPF_6$/EC–EMC solutions: (1) synthetic KS15 graphite electrodes, *C*/4 at 80 °C; (2) MCMB + MCF, *C*/8 at 60 °C; (3) MCMB + MCF, 13.7 mg, *C*/8 at 80 °C.

of life. The coin cells were then opened in a fully discharged state in a glove box. Both the cathode ($LiCoO_2$) and the anode (MCMB + MCF) were removed from the cells. Pairs of such electrodes were tested in coin-type cells: (MCMB + MCF/Li and $LiCoO_2$/Li were prepared with a fresh electrolyte solution). The galvanostatic cycling of these individual electrodes was performed with the same rate (*C*/8). The results are shown in Fig. 1b. While the $LiCoO_2$ electrodes could continue to work, the carbon electrode demonstrated a very quick capacity loss after only several cycles. Thus, it is clear that the anodes are responsible for the capacity fading of the full cells that we studied herein, similar to what was reported earlier for similar systems [7,8]. In order to find out whether such poor high temperature performance is an inherent characteristic of the specific type of the graphitic active mass used in the experiments described in Fig. 1, we compared the cycling behavior of MCMB–MCF electrodes at elevated temperatures to that of electrodes comprised of synthetic KS15 graphite flakes (Fig. 2). Fig. 2 presents the data of an electrode comprised of KS15 graphite flakes cycled at 80 °C with MCMB–MCF electrodes cycled at 60 and 80 °C. The difference in performance between these two types of electrodes is striking. While stable behavior was measured with the KS15 carbon flake electrodes for a period of more than 120 cycles at 80 °C, a pronounced capacity fading was recorded for MCMB–MCF electrodes at both 60 and 80 °C. XRD measurements of cycled electrodes revealed that no structural degradation occurred in either the case of KS15 flakes and or MCMB–MCF graphite electrodes after cycling at 60–80 °C (Table 1). For instance, both the main graphite diffraction peak (0 0 2) position and its FWHM values remained practically invariant when we compared cycled electrodes to pristine ones. Thus, the most probable reason for the drastic capacity fading of MCMB + MCF anodes should be related to surface resistance growth.

After being cycled at elevated temperatures, MCMB + MCF and KS15 graphite electrodes were examined by SEM. Fig. 3 shows typical images of the morphology of pristine (a, c, e and g) and cycled (b, d, f and h) electrodes. The structure and morphology of the surface films deposited on the surfaces of cycled

Table 1
XRD position (2θ) for the 0 0 2 diffraction peak of graphite for pristine electrodes after being cycled at elevated temperatures

Electrode	Peak position, 2θ (°)	FWHM (°)
MCMB + MCF, pristine	26.512	0.254
MCMB + MCF cycled at 60 °C in a half cell	26.556	0.260
MCMB + MCF cycled at 80 °C in a half cell	26.519	0.251
MCMB + MCF cycled at 60 °C in a full cell	26.478	0.272
Synthetic graphite KS15, pristine	26.533	0.246
Synthetic graphite KS15 cycled at 80 °C in a half cell	26.545	0.254

MCMB + MCF and KS15 graphite electrodes differ drastically. There are no pronounced visible changes after high temperature cycling in the morphology of the synthetic graphite flakes oriented with their basal planes parallel to the current collector. The images of pristine and cycled KS15 electrodes (e and f) are very similar, and only at higher magnification (g and h) can one see some evidence for the formation of a thin film with nanoscale particles on the basal planes of the graphite flakes. In contrast, thick microscale deposits are observed on the surface of MCMB–MCF electrodes (b and d), which coat substantial areas of the electrodes' surface. These deposits do not surround each individual graphite particle, but, rather, completely fill the space among the round-shaped particles, thus forming agglomerates with cracks.

Fig. 4a compares a typical Raman spectrum of a MCMB + MCF electrode after being cycled at 60 °C in a half cell (versus Li), recorded at the location of thick surface films with a spectrum of the pristine electrode (Fig. 4b and a, respectively). The typical expected peaks of graphite are marked with asterisks, and peaks attributed to surface species are shown in the insert. A series of bands in the regions of 750–850 and 1050–1200 cm^{-1} may be assigned to the P–O stretching vibrations of meta- and pyrophosphates and PO_xF_y species [14,15], arising from $LiPF_6$ salt decomposition at elevated temperatures.

The presence of PO_4^{3-} as a component in surface films formed on carbon electrodes during storage of Li-ion cells at temperatures above 50 °C was detected by FTIR [16]. The IR peaks, attributed to phosphate (900–1100 cm^{-1}), were found to increase as the storage temperature was higher. Kostecki and McLarnon [17] studied the surface film formation on natural graphite electrodes, cycled at 60 °C, and assigned a series of bands between 1100 and 1150 cm^{-1} to vibrations of (–PO_2) and (–PO_3) groups that belong to surface polyphosphates.

It is possible that polymeric organic species are also present in the surface films formed on carbon electrodes in these systems. The presence of organic species is confirmed by the C–H stretching bands at about 2900 cm^{-1}, together with the C–H deformation bands at about 1400 cm^{-1} in spectrum b of Fig. 4. PEO has its backbone stretching vibration bands around 800–860 cm^{-1} [18], and so the peaks observed in this region may be assigned to these polymeric species. In a similar way, the band at 1180 cm^{-1} may be assigned to the O–C–O stretching vibration of polycarbonates [19].

A Raman spectrum of a MCMB + MCF electrode after being cycled at 60 °C in a full MCMB + MCF/$LiCoO_2$ cell is shown

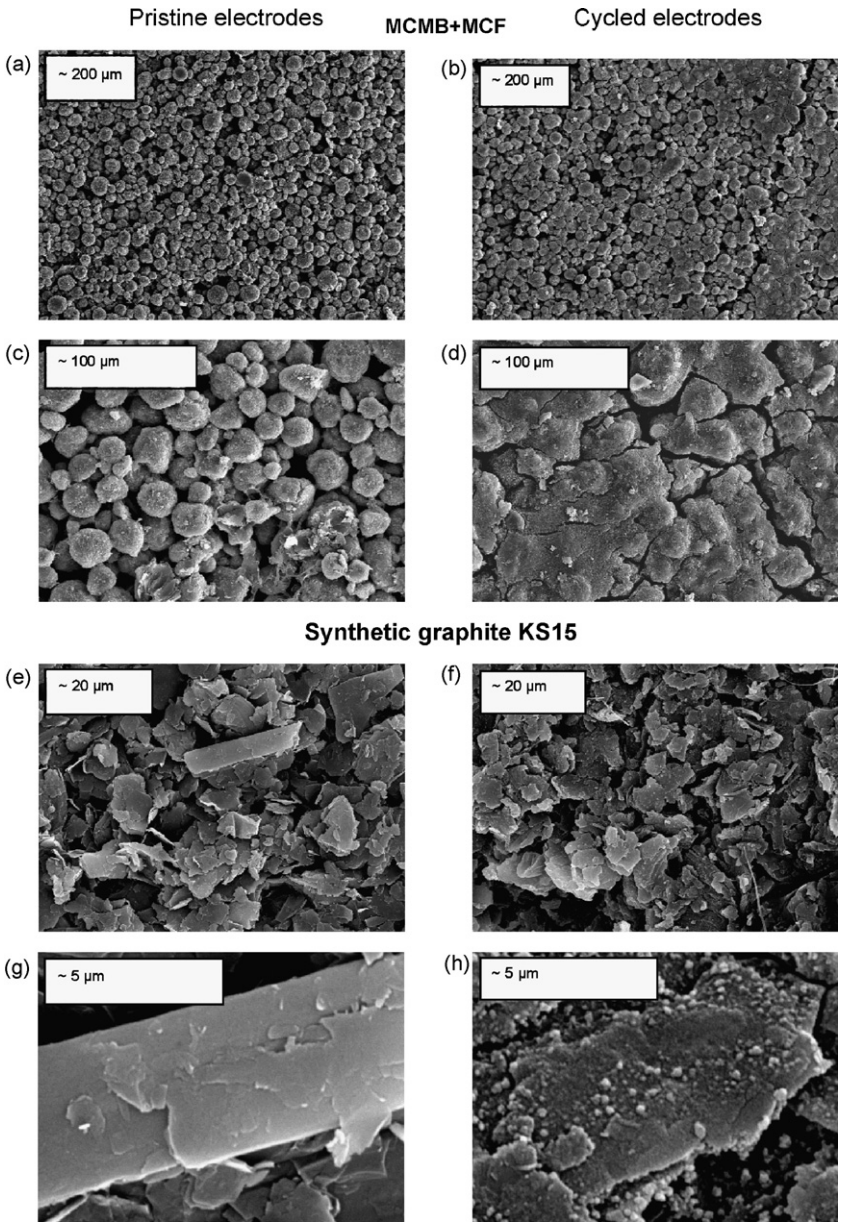

Fig. 3. SEM images of MCMB + MCF and KS15 composite electrodes: (a and c) MCMB + MCF pristine electrode; (b and d) the same electrode after 100 galvanostatic cycles at 60 °C in a MCMB + MCF/Li cell; (e and g) synthetic graphite KS15 pristine electrode; (f and h) the same electrode after 160 galvanostatic cycles at 80 °C in a graphite/Li cell. A scale appears in each micrograph.

in Fig. 5a. Two main peaks dominate the spectrum, which were assigned to lithium carbonate (1091 cm^{-1}, see spectrum b of Fig. 5), and lithium oxalate (1488 cm^{-1}, see spectrum c of Fig. 5) species. As can be seen in the fine details of the spectra in Fig. 4, these species may also be present in the surface films formed on MCMB + MCF electrodes cycled in half cells.

In contrast to the MCMB + MCF electrodes, no additional features, other than graphite peaks, were observed in the Raman spectra of synthetic graphite (KS15) electrodes after being cycled at 80 °C and by probing tens of different locations on the electrodes' surface in each set of measurements (Fig. 6).

Hence, it is clear that the surface films which are obviously formed on these electrodes are too thin to be detected by Raman spectroscopy. In fact, the surface chemistry of carbon electrodes in alkyl carbonates/$LiPF_6$ solutions was studied extensively by us by FTIR spectroscopy and XPS [20,21]. Our findings show that initially, the surface films formed on carbon electrodes in alkyl carbonate-based studies are comprised of Li alkyl carbonates ($ROCO_2Li$) species. Li alkyl carbonates may be replaced by LiF due to secondary reactions with HF. In addition, in the presence of H_2O or at elevated temperatures, they decompose to Li_2CO_3, ROH, and CO_2. Li_xPF_y and Li_xPOF_y surface species are also formed when the salt is $LiPF_6$. Hence, evidence by Raman spectroscopy of the presence of Li_2CO_3 in the surface films formed on MCMB + MCF electrodes is expected. An interesting find is evidence regarding the formation of Li oxalate in the surface films on carbon electrodes, which is in line with the

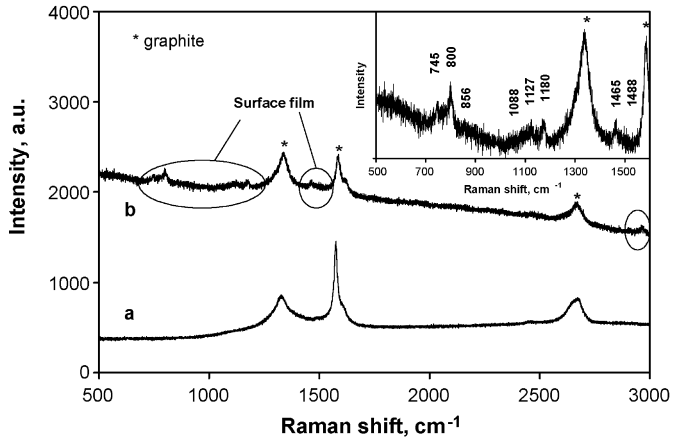

Fig. 4. Raman spectra of a pristine composite graphite electrode MCMB + MCF (a) and of the same electrode after 160 galvanostatic cycles in 1 M $LiPF_6$/EC–EMC at 80 °C (b). The insert shows the enlarged low frequency part of spectrum b.

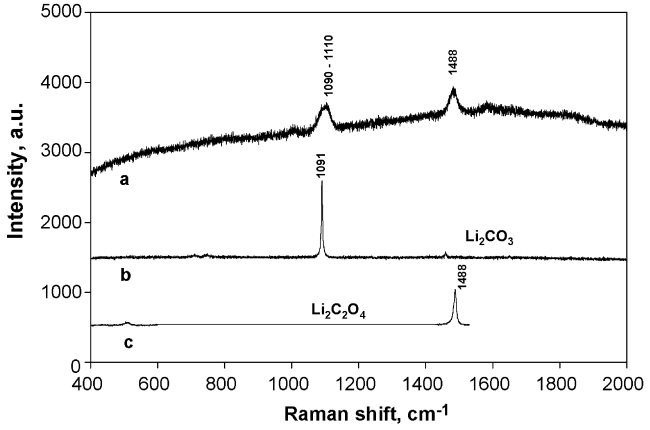

Fig. 5. A Raman spectrum of a MCMB–MCF graphite electrode after being cycled at 60 °C in a $LiCoO_2$/MCMB + MCF cell. Reference Raman spectra of Li carbonate and Li oxalate are also presented for comparison, as indicated.

conclusion of Ross and co-workers [22,23]. Li oxalate can be formed by the reductive decomposition of Li alkyl carbonates, which is expected to occur on Li-carbon surfaces:

$$ROCO_2Li + Li^+ + e^- \rightarrow ROLi + {}^{\bullet}CO_2Li$$

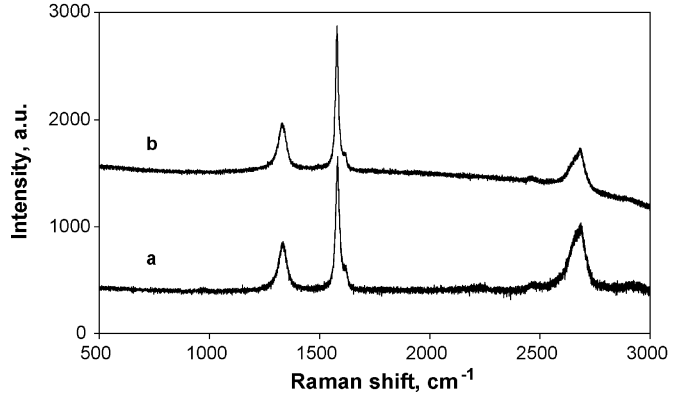

Fig. 6. (a) Raman spectra of a pristine graphite electrode comprised of KS15 synthetic flakes, and (b) of the same electrode after 200 galvanostatic cycles in 1 M $LiPF_6$/EC–EMC at 80 °C.

Coupling of lithiated carboxyl radicals should form Li oxalate. The electrodes cycled in full cells show more pronounced Raman peaks, compared to the electrodes cycled in half (C/Li) cells, because in the latter case the presence of a Li electrode may have an influence on the electrolyte solutions (as a scavenger of active species), and thereby influences the surface chemistry developed on the carbon electrodes. However, a detailed discussion of such impacts is beyond the scope of this paper.

Impedance spectroscopic studies were carried out using coin-type cells with a three-electrode configuration. Fig. 7a presents impedance spectra (Nyquist plots) measured after the initial Li intercalation into the MCMB + MCF anode (1) and after the first deintercalation process (2). The drastic shrinkage of the high frequency semicircle of these spectra after deintercalation during initial cycling of graphite electrodes, has already been described [24,25]. This effect was assigned [25] to the

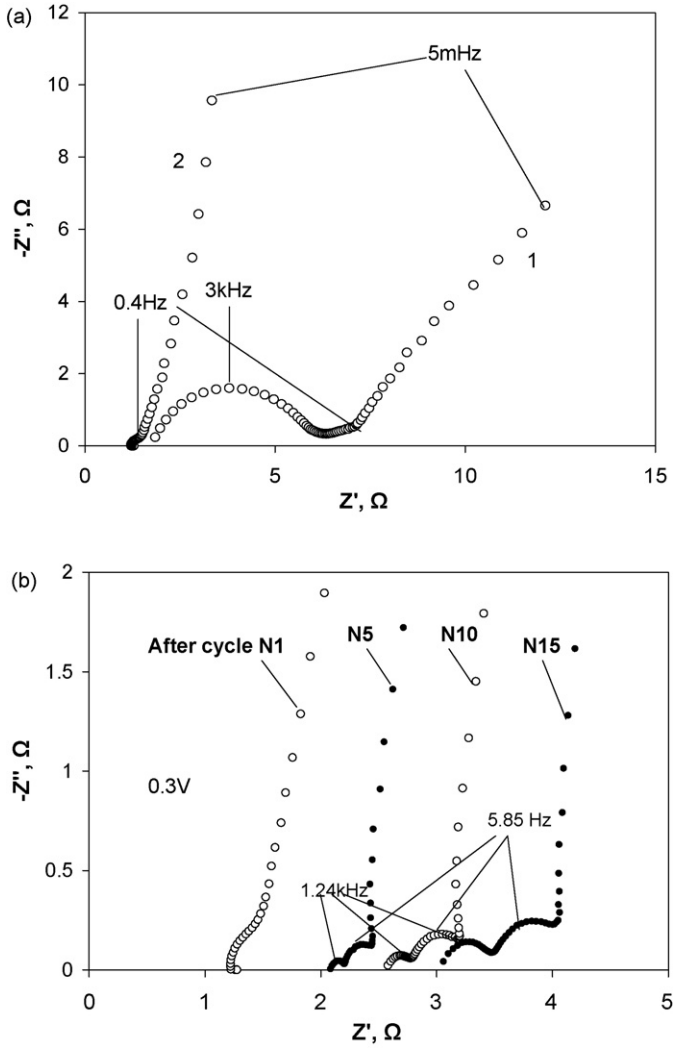

Fig. 7. Impedance spectra of a MCMB + MCF electrode cycled at 60 °C: (a) spectra measured during the first Li intercalation–deintercalation cycle. (1) A spectrum measured at 0.030 V vs. Li/Li^+ after the first lithiation and (2) a spectrum measured at 0.3 V vs. Li/Li^+ after the first delithiation process. (b) Spectra measured at 0.3 V after the 1st, 5th, 10th and 15th cycles, as indicated.

inadequate elastic properties of the initial surface films, which was disrupted as a result of a small shrinkage of the graphite particles during deintercalation. This disruption of the initially formed surface films improves their Li ion transport properties, which leads to a decrease in high frequency impedance. These channels are blocked by precipitation of solution reduction products upon further intercalation, with a repeated significant growth of the high frequency impedance. This periodic shrinkage/growth of the high frequency impedance is seen only in the first lithiation–delithiation cycles of graphite electrodes. As the reformation of the surface films progresses, they become more stable and flexible, and eventually the electrodes' impedance stabilizes upon prolonged cycling and hence, only slightly depends on the potential [25]. Thus, one can expect that the thicker and less flexible the surface films, the more pronounced is the shrinkage/growth of the high frequency impedance during the initial cycling of graphite electrodes. Indeed, the behavior presented in Fig. 7a, related to the initial cycling of MCMB + MCF electrodes, reflects remarkable changes in the electrode's impedance upon intercalation–deintercalation. Similar measurements of an electrode comprised of synthetic graphite flakes (much thinner surface films) showed that the difference in impedance between intercalated–deintercalated states is much less pronounced, as compared to the MCMB + MCF electrodes [25]. Fig. 7b shows a series of Nyquist plots measured at 0.3 V (deintercalated state) during the cycling of a MCMB + MCF electrode at 60 °C. The cycle numbers are indicated. It can be clearly seen that due to cycling, the solution resistance increases, the high frequency semicircle increases, and a new medium frequency semicircle appears and grows (upon cycling). These changes in the electrode's impedance upon cycling are in line with all other observations: the pronounced capacity fading and the thickening of the surface films.

It is remarkable that despite the fact that MCMB + MCF electrodes rapidly develop thick surface layers during cycling at elevated temperatures, they possess a lower initial irreversible capacity compared to that of synthetic graphite electrodes (Table 2). This can be explained by the fact that the surface area of the KS15 graphite is higher than that of MCMB and MCF (BET area measured for KS15 was 11.6 $m^2 g^{-1}$, while for a MCMB + MCF mixture it was 1.3 $m^2 g^{-1}$). Thus, the irreversible capacity of these electrodes correlates approximately with their BET surface areas, and thus, these electrodes have the same irreversible capacity per unit surface area.

All the experimental results presented above converge into a very clear picture. The round-shaped graphite materials, MCMB and MCF, are surface reactive and much more sensitive to the electrolyte solutions, compared to graphite flakes. Based on structural analysis (XRD), it is clear that the rapid capacity fading of MCMB + MCF electrodes at elevated temperatures is not due to the bulk destruction of the active mass (e.g., exfoliation), but rather to the formation of thick surface films that lead to an increased impedance upon cycling. The round-shaped materials mostly have edge planes at their surfaces, in contrast to flakes whose surface area contains basal planes, in at least half of their surface envelopes. The edge planes may be more reactive towards solution species than basal planes, and some evidence does exist for this [26,27]. Hence, at least in part, the thick surface films formed on MCMB + MCF electrodes may be due to the relatively high reactivity of the entire surface area of the particles. However, there may be other important reasons for the difference between MCMB and flakes. As already demonstrated by us [28] and by others [17,29], even in the best electrolyte solutions, graphite particles undergo some amorphization near their surfaces during prolonged cycling. There are small-scale destructive processes that increase the surface area of the particles by fractures and microexfoliation, as has been explained [28]. Such destructive processes are expected to occur mostly on edge planes. The MCMB–MCF particles, whose surface includes mostly edge planes, should be much more sensitive to the above destructive processes. Increasing the surface area of the graphite particles upon cycling should obviously lead to insufficient passivation and continuous reactions between the active mass and the solution species, to form surface films that become increasingly thicker. Such a scenario explains all of the results presented above.

Table 2
Initial irreversible capacity of graphite electrodes in graphite/Li cells

Electrode	Temperature (°C)	Rate	Irreversible capacity (%)
MCMB + MCF	60	*C*/8	6.9
MCMB + MCF	80	*C*/8	8.9
Synthetic graphite KS15	80	*C*/4	31.6

4. Conclusions

Graphite electrodes comprised of synthetic flakes may demonstrate impressive stability at elevated temperatures (up to 80 °C) in standard solutions, e.g., $LiPF_6$-EC/EMC. Capacities close to the theoretical one (372 mAh g^{-1}) could be measured at 80 °C over a period of more than 120 cycles (completed lithiation–delithiation). In contrast, electrodes comprised of round-shaped particles (MCMB) and chopped carbon fibers (MCF) demonstrated rapid capacity fading at elevated temperatures. The low performance observed for the latter material is not due to bulk structure instability upon cycling, but rather to pronounced surface solutions at elevated temperatures with solution species, which lead to the formation of thick surface films that increase remarkably the electrodes' impedance upon cycling (which in turn causes the observed capacity fading). These surface films contain Li_2CO_3 and Li oxalate, as is clearly evidenced by Raman spectroscopy.

The thick surface films are developed on MCMB and MCF particles because their surface includes mostly edge planes, which are more reactive towards solution species than are basal planes (that make up a great part of the surface of graphite flakes). The round-shaped particles are more sensitive to the destructive processes of microscale graphite, near the surface when it undergoes repeated and prolonged lithiation–delithiation cycling. This destruction process worsens the passivation of the electrodes upon cycling, and thereby allows continuous surface reactions that form thick surface films.

References

[1] Y. Matsuo, R. Kostecki, F. McLarnon, J. Electrochem. Soc. 148 (2001) A687–A692.
[2] T. Eriksson, A. Andersson, C. Geike, T. Gustafsson, J. Thomas, Langmuir 18 (2002) 3609–3619.
[3] K. Stribel, J. Shim, E. Cairns, R. Kostecki, Y.-J. Lee, J. Reimer, T. Richardson, P. Ross, X. Song, G. Zhuang, J. Electrochem. Soc. 151 (2004) A857–A866.
[4] J. Shim, R. Kostecki, T. Richardson, X. Song, K. Stribel, J. Power Sources 112 (2002) 222–230.
[5] K. Amine, C. Chen, J. Liu, M. Hammond, A. Jansen, D. Dees, I. Bloom, D. Vissers, G. Henriksen, J. Power Sources 97–98 (2002) 684–687.
[6] D. Zhang, B. Haran, A. Durairajan, R. White, Y. Podrazhansky, B. Popov, J. Power Sources 91 (2000) 122–129.
[7] P. Ramadass, B. Haran, R. White, B. Popov, J. Power Sources 112 (2002) 606–613.
[8] P. Ramadass, B. Haran, R. White, B. Popov, J. Power Sources 112 (2002) 614–620.
[9] D. Aurbach, H. Teller, M. Koltypin, E. Levi, J. Power Sources 119–121 (2003) 2–7.
[10] D. Aurbach, H. Teller, E. Levi, J. Electrochem. Soc. 149 (2002) A1255–A1266.
[11] M. Winter, K.-C. Moeller, J.O. Besenhard, in: G.-A. Nazri, P. Gianfranco (Eds.), Lithium Batteries, Kluwer Academic Publishers, Norwell, MA, 2004, pp. 144–194.
[12] M.D. Levi, D. Aurbach, J. Phys. Chem. B 101 (1997) 4630–4640.
[13] M.D. Levi, C. Wang, D. Aurbach, Z. Chvoj, J. Electroanal. Chem. 562 (2004) 187–203.
[14] L. Popovic, D. de Waal, J.C.A. Boeyens, J. Raman Spectrosc. 36 (2005) 2–11.
[15] L. Zhang, L. Wen, J. Zhang, L. Hu, Mater. Chem. Phys. 91 (2005) 166–171.
[16] K. Araki, N. Sato, J. Power Sources 124 (2003) 124–132.
[17] R. Kostecki, F. McLarnon, J. Power Sources 119–121 (2003) 550–554.
[18] X. Yang, Z. Su, D. Wu, S.L. Hsu, H.D. Stidham, Macromolecules 30 (1997) 3796–3802.
[19] J. Flores, E. Chronister, J. Raman Spectrosc. 27 (1996) 149–153.
[20] D. Aurbach, B. Markovsky, A. Shechter, Y. Ein-Eli, H. Cohen, J. Electrochem. Soc. 143 (1996) 3809–3820.
[21] D. Aurbach, B. Markovsky, I. Weissman, E. Levi, Y. Ein-Eli, Electrochim. Acta 45 (1999) 67–86.
[22] G.V. Zhuang, P.N. Ross Jr., Electrochem. Solid State Lett. 6 (2003) A136–A139.
[23] A. Augustsson, M. Herstedt, J.-H. Guo, K. Edström, G.V. Zhuang, P.N. Ross Jr., J.-E. Rubensson, J. Nordgren, Phys. Chem. Chem. Phys. 6 (2004) 4185–4189.
[24] M. Holzapfel, A. Martinent, F. Alloin, B. Le Gorrec, R. Yazami, C. Montella, J. Electroanal. Chem. 546 (2003) 41–50.
[25] E. Markevich, M.D. Levi, D. Aurbach, J. Electrochem. Soc. 152 (2005) A778–A786.
[26] E. Peled, D. Bar Tow, A. Merson, A. Gladkich, L. Burstein, D. Golodnitsky, J. Power Sources 97–98 (2001) 52–57.
[27] E. Peled, D. Golodnitsky, A. Ulus, V. Yufit, Electrochim. Acta 50 (2004) 391–395.
[28] E. Markevich, G. Salitra, M.D. Levi, D. Aurbach, J. Power Sources 146 (2005) 146–150.
[29] Q. Pan, K. Guo, L. Wang, S. Fang, J. Mater. Chem. 12 (2002) 1833–1838.